Detection of Aggressive Primary Prostate Cancer with ^{11}C-Choline PET/CT Using Multimodality Fusion Techniques

Morand Piert[1], Hyunjin Park[1], Asra Khan[1], Javed Siddiqui[2], Hero Hussain[1], Thomas Chenevert[1], David Wood[3], Timothy Johnson[4], Rajal B. Shah[2], and Charles Meyer[1]

[1]Department of Radiology, University of Michigan, Ann Arbor, Michigan; [2]Department of Pathology, University of Michigan, Ann Arbor, Michigan; [3]Department of Urology, University of Michigan, Ann Arbor, Michigan; and [4]Department of Biostatistics, University of Michigan, Ann Arbor, Michigan

The aim of the study was to assess whether ^{11}C-choline PET/CT could identify high-risk primary adenocarcinoma of the prostate. **Methods:** ^{11}C-choline PET/CT and transpelvic MRI were performed in 14 patients with untreated localized primary adenocarcinoma of the prostate, followed by radical prostatectomy as a form of primary monotherapy within 14 d of in vivo imaging. To allow accurate coregistration of whole-mount histology with in vivo imaging, additional ex vivo MR images of the prostatectomy specimen were obtained. Nonlinear 3-dimensional image deformations were used for registrations of PET/CT, MRI, and histology. Volumes of interest from tumor and benign tissue were defined on the basis of histology and were transferred into coregistered ^{11}C-choline PET/CT volumes to calculate the mean ($T_{(mean)}$/B) and maximum ($T_{(max)}$/B) ratio of tumor to benign prostate background. On the basis of MIB-1/Ki-67 expression in tumor tissues represented on a tissue microarray, we assessed whether ^{11}C-choline uptake correlated with local Gleason score and tumor proliferation. **Results:** Histology confirmed 42 tumor nodules with Gleason scores between 3 + 2 and 4 + 4, with volumes ranging from 0.03 to 12.6 cm^3. $T_{(mean)}$/B ($P < 0.01$) and $T_{(max)}$/B ($P < 0.001$) ratios were significantly increased in high–Gleason score (≥4 + 3) lesions versus 3 + 4 and lower disease but failed to distinguish between 3 + 4 disease versus 3 + 3 and lower. $T_{(mean)}$/B and $T_{(max)}$/B ratios were significantly increased in tumors with an MIB-1/Ki-67 labeling index greater than or equal to 5% ($P < 0.01$). **Conclusion:** On the basis of our preliminary data using ratios of tumor to benign prostate background, ^{11}C-choline preferentially identified aggressive primary prostate cancer.

Key Words: ^{11}C-choline; PET/CT; PET/MRI; primary prostate cancer; image fusion

J Nucl Med 2009; 50:1585–1593
DOI: 10.2967/jnumed.109.063396

Received Feb. 19, 2009; revision accepted Jun. 29, 2009.
For correspondence or reprints contact: Morand Piert, University of Michigan Health System, Department of Radiology, Division of Nuclear Medicine, University Hospital, B1G505C, 1500 E. Medical Center Dr., Ann Arbor, MI 48109-0028.
E-mail: mpiert@umich.edu

There is no consensus on what criteria should be used to initiate definitive treatment (such as surgery or radiation therapy) in men undergoing active surveillance for known localized adenocarcinoma of the prostate. A recent update on the results of the randomized trial comparing radical prostatectomy versus watchful waiting in localized prostate cancer performed by the Scandinavian Prostate Cancer Group (study 4) indicated that prostatectomy did not prolong survival unless patients were younger than 65 y (*1*). However, this study also showed that in those patients who received prostatectomy the disease-related mortality clearly increased with high Gleason scores. Identifying aggressive disease early in the disease process could, therefore, be beneficial for therapeutic decision making (*2*).

The current diagnostic situation is, however, unsatisfactory because many prostate cancers represent clinically irrelevant disease, and the diagnosis poses the risk for overtreatment. Especially in the light of the known side effects of localized treatment, this is a difficult clinical and ethical dilemma. The standard of care is repeated random prostate biopsy, which—because of sampling errors—frequently under- or overestimates the true Gleason pattern as determined from prostatectomy specimens (*3,4*). Because of this dilemma, the initiation of treatment is often influenced by the individual preferences of the patient but generally includes palpable tumors with a Gleason score of at least 7 in several biopsies or any tumor biopsy with a Gleason score greater than 7.

Hybrid PET/CT with ^{11}C-choline has shown promise in the detection of primary prostate cancer associated with upregulated choline kinase activity and increased choline retention. Choline is incorporated into phosphatidylcholine, a major component of cell membranes. Malignant tumors show increased proliferation and metabolism of cell membrane components and, accordingly, an increased choline uptake (*5*). Thus far, studies evaluating ^{11}C-choline for the detection of primary prostate cancer have been inconclusive (*6–9*). Some encouraging recent reports from Scher et al.

(*10*) and Krause et al. (*11*) indicated that detection rates in recurrent disease are related to the disease burden as assessed by prostate-specific antigen (PSA) values. However, to date all studies comparing ^{11}C-choline imaging results with histology, whether from biopsies or prostatectomy specimens, suffer from considerable uncertainty about the true location of disease in relation to the imaging findings they are felt to represent.

To minimize these technical limitations, we compared ^{11}C-choline PET/CT with histologic truth using a rigorous, nonbiased, coregistration method with a standard mutual-information cost-function algorithm and thin-plate spline (TPS) warping (*12*). This registration technique—using high-resolution ex vivo MRI of the prostatectomy specimen and whole-mount histology—allowed us to assess the ability to detect primary prostate cancer and evaluate whether imaging would correlate with histologic features associated with tumor aggressiveness. We selected the well-established Gleason score and immunostaining for MIB-1/Ki-67, a nuclear protein complex expressed during cell replication, as surrogate markers for aggressiveness; both have been shown to be reliable prognostic markers in prostatectomized patients (*13–15*).

MATERIALS AND METHODS

Patient Population

The study was conducted in 14 men (mean age, 59.6 y; range, 47–72 y) with biopsy-proven, untreated localized adenocarcinoma of the prostate scheduled for prostatectomy (Table 1). Eligible patients received prostate biopsies (6 samples from each lobe) within 16 wk before enrollment, which resulted in 3 or more cores with a Gleason score of 6 or greater from at least 1 lobe of the prostate. A negative bone scan result and a CT scan of the abdomen and pelvis were required if the PSA level was greater than or equal to 15 ng/mL or if a biopsy Gleason score greater than or equal to 8 was obtained. Patients with prior androgen ablation treatment, prostate biopsies performed less than 6 wk before PET/CT and MRI, previous external radiation treatment of the pelvic region, any prior malignancies, active inflammatory bowel disease, or evidence of prostatitis were not eligible.

In Vivo Imaging

In vivo imaging was performed within 14 d before radical prostatectomy (mean, 7.4 d; range, 3–14 d). In 11 cases, MRI and ^{11}C-choline PET/CT were performed on the same day, whereas in the remaining 3 cases imaging was completed 1 d apart. MRI was performed to allow for subsequent image coregistration and identification of focal prostate lesions. Therefore, MRI included anatomic T2-weighted 3-T MRI (Achieva; Philips) using a transpelvic coil. Scans were obtained in the axial orientation using a high-resolution sequence with a repetition time of 3,208 ms and an echo time of 86 ms. Images were reconstructed in a 720 × 720 × 24 pixel matrix, resulting in a 0.31 × 0.31 × 4 mm voxel dimension with an echo time of 4,151 ms and a repetition time of 90 ms.

PET/CT was performed on a Siemens Biograph classic scanner, which incorporates an ECAT HR+ PET camera with a 2-channel helical CT camera (n = 12). In 2 cases, PET/CT was performed on a Biograph TrueV HiRez scanner with extended field of view and a 6-channel helical CT camera (Siemens Medical Solutions). The intrinsic axial resolution of these 2 PET/CT systems (at the center of the field of view) differs, with approximately 5.2 mm in full width at half maximum (FWHM) for the first (*16*) and 4.5 mm in FWHM for the second scanner. After injecting approximately 700 MBq of ^{11}C-choline, we obtained a limited body scan of the abdomen and pelvis, starting 5 min after injection (*6,8,17*) at the level of the prostate (7 min/bed position). Images were reconstructed in a 128 × 128 × 210 matrix, resulting in a 5.2 × 5.2 × 2.4 mm voxel dimension using identical iterative (ordered-subset expectation maximum) algorithms on both scanners (Fourier rebinning; 4 iterations, 8 subsets), with a 7-mm gaussian filter using low-dose CT without intravenous or oral contrast for attenuation correction. As a result, the effective axial reconstructed resolution was similar on both scanners and determined to be approximately 9.0 mm in FWHM on the first and 8.5 mm in

TABLE 1. Patient Characteristics

Patient no.	Age (y)	^{11}C-choline injected activity (MBq)	PSA (ng/mL)	Prostate weight (g)	T-stage, final pathology	Highest Gleason score	
						Biopsy	Final pathology
1	47	706.7	10.1	27.4	T2b	3 + 4	3 + 4
2	72	725.2	8.7	40.9	T3a	4 + 3	3 + 4
3	60	728.9	8.5	45.1	T3a	4 + 3	4 + 3
4	56	669.7	7.1	52.8	T2b	4 + 4	4 + 3
5	59	691.9	12.1	49.1	T3b	3 + 4	4 + 4
6	59	658.6	17.9	63.0	T3b	3 + 4	4 + 4
7	64	684.5	2.2	64.5	T2b	3 + 3	3 + 4
8	66	651.2	5.9	41.2	T3a	3 + 4	4 + 3
9	67	721.5	3.9	43.8	T2b	4 + 4	4 + 3
10	64	691.9	10.2	47.7	T3b	3 + 4	4 + 3
11	55	695.6	4.6	41.7	T3a	3 + 4	3 + 4
12	63	666.0	4.4	44.9	T2b	4 + 3	4 + 3
13	46	699.3	6.9	39.7	T2b	3 + 4	3 + 4
14	56	703.0	8.2	45.4	T3a	3 + 3	4 + 3
Mean	59.6	692.4	7.9	46.2			
SD	7.3	24.4	4.0	9.4			

FWHM on the second scanner (Robert Koeppe, oral communication, 2008).

Image Coregistration

A standard registration method based on a mutual-information cost function and TPS deformation was used (*18*). Registration among in vivo imaging modalities is well established, but accurate registration involving histology is challenging. A detailed description of the applied methodology is available (*12*). Briefly, our approach separated the difficult direct registration of histology and in vivo imaging (PET/CT, MRI) into achievable subregistration tasks involving intermediate ex vivo modalities such as block-face photography and specimen MRI, which was performed 2–3 d after prostatectomy. Additional volumetric stacking of block-face photographs (registered with histology) improved registration onto specimen MRI volumes. Results of subregistration tasks were combined to compute the intended, final registration between our reference space (T2-weighted MRI) and whole-mount histology (Fig. 1). Registration errors between in vivo imaging and histology were previously determined to be in the range of 2.26–3.74 mm (*12*).

Histologic Assessment and Tissue Microarray Construction

Fresh prostates were removed after surgery and fixed overnight in 10% neutral formalin. After specimen MRI, the prostate was sectioned at 3-mm intervals perpendicular to the long axis of the gland from the base to apex and processed for histologic assessment (hematoxylin and eosin [HE] stain) using a whole-mount technique (*19,20*). Tumor maps were generated for each whole-mount slice to determine individual tumor foci in multifocal prostate cancers as previously described (*21*). Each tumor focus was assigned a primary and secondary Gleason grade and staged according to the 1998 guidelines of the American Joint Committee on Cancer (*22*). Benign hyperplasia was diffusely present in almost all benign prostatic regions.

A tissue microarray representing a total of 42 tumor foci from 14 patients (which included an index tumor and any separate secondary tumor) and benign tissue was constructed from these prostatectomy specimens. Three cores were taken from each sampled tissue area, resulting in a total of 162 cores available for analysis. Proliferation was determined by the percentage nuclear expression of MIB-1 immunohistochemistry (Dako) on formalin-fixed, paraffin-embedded tissue and quantified by digital image analysis as previously described (*20*). An MIB-1/Ki-67 labeling index of 5% or higher was considered positive (*14*). Histology was evaluated (biopsies, prostatectomy specimen, MIB-1/Ki-67 labeling index) by 1 investigator unaware of the results of PET/CT and MRI.

Image Analysis

Image coregistration of ^{11}C-choline PET with pathology enabled us to compare in vivo imaging results with histologic truth (including local Gleason score and MIB-1/Ki-67 labeling index). First, volumes of interest (VOI) were defined on coregistered consecutive HE pathologic sections, contouring the borders of each tumor lesion individually and thereby calculating the tumor volume. Also, at least 1 standardized VOI (1.5 cm^3) was defined in benign tissue in the peripheral zone and central gland, avoiding proximity to cancerous lesions. VOIs were then evaluated on coregistered ^{11}C-choline PET images to obtain the mean and maximum standardized uptake value (SUV). As a result, the location of the VOI (in 3-dimensional [3D] space) was defined solely by pathology and not by any imaging feature visually identified on PET or MR images.

To minimize the effect of differing PET equipment (especially counting efficacy), PET results were normalized by benign prostate tissue before further analysis. Because almost all nonmalignant regions included areas of diffuse benign hyperplasia, normalization was performed on the basis of a mixture of normal and hyperplastic benign prostatic tissues. We calculated the mean ($T_{(mean)}$/B) and maximum ($T_{(max)}$/B) ratios of tumor to benign prostate background using contralateral histologically benign tissue as reference. Tumor uptake was normalized according to location; thus, peripheral zone tumors were normalized by nonmalignant contralateral peripheral zone tissue. The ^{11}C-choline uptake in larger tumors involving significant portions of the prostate lobe was normalized by the mean of the benign peripheral and central gland (avoiding the inclusion of the urethra in the VOI).

Statistics

Results are expressed as mean values of parameters ± SD. Parameters were compared by means of 1-way ANOVA using the measured tumor volume (below 1 cm^3) as weighting factor, and tumors larger than 1 cm^3 were assessed without weighting. As a result, tumor nodules with volumes below 1 cm^3 contributed progressively less (with decreasing volume) to the result of statistical testing, thereby accounting for a decreasing reliability of the ^{11}C-choline uptake measures with decreasing volume. The homogeneity of group variances was tested using the Levene test at a nominal significance level of 0.1, offering more protection against falsely declaring all variances equal when in fact they were not. In the case of homogeneous group variances, data were compared using a *t* test or paired *t* test, when appropriate. If variances were not equally distributed, group differences were assessed using the Wilcoxon signed rank test. A *P* value of less than 0.05 was considered statistically significant. Statistical tests were performed with the JMP statistical software package (SAS).

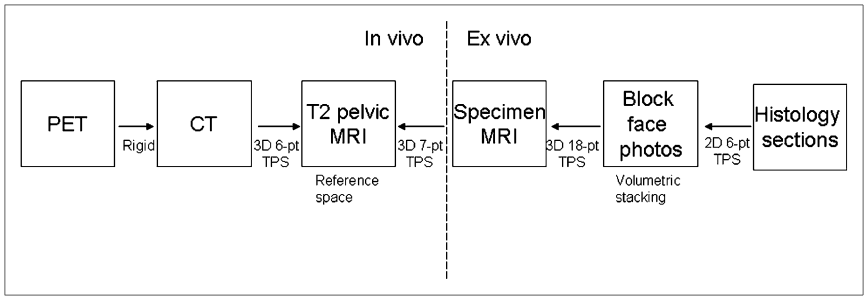

FIGURE 1. 3D images were registered using mutual-information system and TPS deformation with 6–18 points (pts). All registration subtasks (solid arrows) are 3D registrations, except for histology onto block-face registration. Pictures of registered ^{11}C-choline PET, anatomic MRI (references space), ex vivo specimen MRI, and respective histology section are provided in Figure 3.

RESULTS

Table 1 summarizes patient data. Patients were staged T2b–T3b at pathology. The mean PSA in our study population was 7.9 ± 4.0 ng/mL (range, 2.2–17.9 ng/mL). The weight of the prostate specimen ranged from 27.4 to 65.4 g.

Table 2 summarizes the results of the 42 tumor nodules identified on HE histology. With the exception of a single case, tumors were generally multifocal, with focal nodule volumes ranging from 0.03 to 12.6 cm^3. Small tumors, below the reconstructed resolution of ^{11}C-choline PET/CT, were in the majority. Therefore, partial-volume effects clearly influenced the ability to characterize disease. To minimize these effects, we used the tumor volume (as determined by fusion imaging with pathology) as a weighting factor, thus accounting for greater reliability of imaging results obtained from larger tumor volumes and down-weighting the effects of unreliable low-volume lesions (<1 cm^3) in the statistical analyses. Gleason scoring of the largest tumor lesion per patient varied between 3 + 3 and 4 + 4. Multifocal (secondary) tumor lesions were generally scored as Gleason 3 + 4 and lower; however, 2 separate satellite 4 + 4 lesions (volumes, 0.3 and 0.4 cm^3) were found in the vicinity of a larger 4 + 4 lesion (patient 6; Table 2), thus clearly reducing the likelihood of detection by PET.

^{11}C-choline uptake was not uniformly distributed within the nonmalignant prostate tissues. The mean ^{11}C-choline SUV of the nonmalignant central gland (mean SUV, 3.1 ± 1.4) was significantly higher ($P < 0.005$) than the respective benign peripheral gland (mean SUV, 2.5 ± 0.4) using paired comparisons within individual patients. To account for these distribution differences, we selected the benign background tissue according to the location of the tumor nodule as described in the "Materials and Methods" section.

Focally increased ^{11}C-choline uptake within the prostate was identified only in tumors; thus, no cases with false-positive findings were observed. Figure 2 shows the PET/CT images of patient 14 with focally increased ^{11}C-choline uptake on the left side of the gland. Figure 3 displays the results of the registrations of ex vivo specimen and in vivo anatomic MRI plus ^{11}C-choline PET/CT onto histology for the same patient. The left-sided tumor (volume, 6.8 cm^3) was graded Gleason 4 + 3, with an MIB-1/Ki-67 labeling index of 12; 2 right-sided low-volume lesions graded Gleason 3 + 3 remained undetected by PET. The axial PET planes in Figures 2 and 3 are not identical, because the respective PET image slice and the prostate specimen MRI and histology slices underwent nonlinear warping to match the transpelvic T2-weighted MRI reference slice in Figure 3.

Volume-weighted ^{11}C-choline $T_{(mean)}$/B and $T_{(max)}$/B ratios were used for further data analyses because these parameters relate to visual identification of potential tumor foci. The $T_{(mean)}$/B ($P < 0.01$) and the $T_{(max)}$/B ($P < 0.001$) ratios were significantly elevated in lesions with a Gleason score of 4 + 3 or higher ($T_{(mean)}$/B, 1.5 ± 0.5; $T_{(max)}$/B, 2.4 ± 0.9) versus 3 + 4 and lower ($T_{(mean)}$/B, 0.9 ± 0.2; $T_{(max)}$/B, 1.4 ± 0.2). However, there was considerable overlap between these groups. Also, the $T_{(mean)}$/B and $T_{(max)}$/B ratios failed to distinguish Gleason 3 + 4 ($T_{(mean)}$/B, 0.9 ± 0.2; $T_{(max)}$/B, 1.4 ± 0.3) versus less than or equal to 3 + 3 disease ($T_{(mean)}$/B, 0.9 ± 0.1; $T_{(max)}$/B, 1.4 ± 0.2) because such tumors generally showed ^{11}C-choline uptake similar to benign prostate (Fig. 4). On the other hand, the mean SUV of the tumor tissue (Gleason score ≥ 4 + 3: 4.0 ± 1.8; Gleason score ≤ 3 + 4: 2.8 ± 1.3) did not correlate significantly with Gleason scoring ($P = 0.22$).

We repeated this analysis in a subgroup with tumor volumes greater than 1 cm^3 ($n = 16$). Again, the data showed that the $T_{(mean)}$/B ratio ($P < 0.01$) and the $T_{(max)}$/B ratio ($P < 0.01$) differentiated tumors with a Gleason score of 4 + 3 or higher ($T_{(mean)}$/B, 1.6 ± 0.5; $T_{(max)}$/B, 2.6 ± 1.0) versus 3 + 4 and lower ($T_{(mean)}$/B, 0.9 ± 0.2; $T_{(max)}$/B, 1.4 ± 0.3), indicating that mere partial-volume effects did not explain the overall findings. Tumors with extracapsular extension (T3 lesions: penetration of the prostatic capsule or seminal vesicle invasion, $n = 11$; $T_{(mean)}$/B, 1.4 ± 0.5; $T_{(max)}$/B, 2.3 ± 1.0) displayed significantly higher $T_{(mean)}$/B ($P < 0.001$) and $T_{(max)}$/B ($P < 0.001$) ratios than did the remaining lesions ($T_{(mean)}$/B, 1.0 ± 0.3; $T_{(max)}$/B, 1.3 ± 0.4; $n = 31$). However, extracapsular extension was never directly identified on ^{11}C-choline PET images.

The MIB-1/Ki-67 labeling indices were generally low; however, they increased with higher Gleason scores (Table 2). We found significantly higher MIB-1/Ki-67 labeling indices with primary Gleason scores of 4 + 3 and higher (10.9 ± 9.4) than with 3 + 4 and lower (0.8 ± 0.9; $P < 0.01$), indicating that both histologic markers are linked with each other ($n = 42$). Also, the ^{11}C-choline $T_{(mean)}$/B ($P < 0.01$) and the $T_{(max)}$/B ($P < 0.01$) ratios were significantly higher in tumors showing elevated MIB-1/Ki-67 labeling indices greater than or equal to 5 ($T_{(mean)}$/B, 1.7 ± 0.6; $T_{(max)}$/B, 2.7 ± 1.1) than in lesions with an MIB-1/Ki-67 labeling index less than or equal to 4 ($T_{(mean)}$/B, 1.0 ± 0.2; $T_{(max)}$/B, 1.5 ± 0.3). These data indicate that the ^{11}C-choline tumor uptake increased with moderately rising proliferation indices (Fig. 5). The mean tumor SUV did not correlate with MIB-1/Ki-67 ($P = 0.68$). MIB-1/Ki-67 staining was negative in all sampled benign tissues.

In addition, we evaluated the value of the prostate biopsies for the prediction of the final Gleason score. Because the true location of the individual prostate biopsy (within a given lobe) was not known, we compared the maximum Gleason score of each prostate lobe obtained from biopsies with the final specimen ($n = 27$). In 6 cases, no tumor was identified by biopsies in prostate lobes bearing tumor at final pathology. However, these cases were exclusively tumors with a final Gleason score of 3 + 3 or lower. Nevertheless, the biopsies failed to accurately predict the final primary Gleason score to be 4 + 3 and higher versus 3 + 4 and lower ($P = 0.16$).

TABLE 2. Characteristics of Individual Tumor Nodules

Tumor no.	Patient no.	Tumor volume (mm^3)	Gleason score	MIB-1/Ki-67 labeling index	Mean tumor SUV	Maximum tumor SUV	$T_{(mean)}$/B ratio	$T_{(max)}$/B ratio
1	1	853	3 + 4	0	3.4	4.4	1.3	1.6
2	1	1,501	3 + 4	0	2.0	2.2	0.7	0.8
3	1	973	3 + 3	3	3.1	4.4	1.2	1.6
4	2	1,741	3 + 4	0	1.4	2.3	1.0	1.5
5	2	64	3 + 3	0	1.4	1.5	0.9	1.0
6	2	255	3 + 3	0	1.5	2.0	1.0	1.4
7	2	66	3 + 3	6	1.8	2.1	1.2	1.4
8	3	2,587	4 + 3	0	3.6	5.1	1.1	2.0
9	3	63	3 + 3	0	2.2	2.4	0.7	0.8
10	3	335	3 + 3	0	4.0	4.6	1.3	1.4
11	3	351	3 + 3	2	2.6	3.4	0.9	1.1
12	4	817	4 + 3	12	3.2	3.8	1.1	1.3
13	4	61	3 + 3	0	2.9	3.1	1.0	1.1
14	5	7,166	4 + 4	24	1.7	2.8	1.0	1.7
15	6	9,861	4 + 4	30	4.0	6.3	1.7	2.7
16	6	340	4 + 4	3	2.7	3.4	1.2	1.5
17	6	399	4 + 4	0	3.4	3.9	1.3	1.5
18	7	3,982	3 + 4	3	1.2	1.9	0.8	1.2
19	7	679	3 + 3	0	2.0	2.3	0.9	1.1
20	7	53	3 + 3	9	0.9	1.0	0.6	0.6
21	7	75	3 + 3	0	1.1	1.2	0.5	0.8
22	8	1,227	4 + 3	9	3.3	4.6	1.2	1.7
23	8	212	3 + 3	0	2.4	2.6	0.9	1.0
24	9	227	3 + 2	0	1.7	1.8	0.9	0.9
25	9	2,469	4 + 3	4	2.8	5.0	1.4	2.6
26	10	12,627	4 + 3	18	2.3	4.1	2.1	3.8
27	10	132	3 + 2	0	1.2	1.4	1.1	1.3
28	11	1,011	3 + 3	0	1.7	3.1	0.7	1.3
29	11	1,980	3 + 4	0	2.5	4.1	1.0	1.7
30	11	224	3 + 4	4	3.8	4.2	1.3	1.4
31	11	34	3 + 3	0	3.9	4.1	1.3	1.4
32	11	1,518	3 + 3	3	2.8	4.2	1.0	1.4
33	12	3,596	4 + 3	3	1.7	3.3	1.2	2.3
34	12	624	3 + 4	0	1.1	2.3	0.5	1.0
35	12	1,330	3 + 3	0	0.8	2.6	0.6	1.8
36	12	612	4 + 3	0	1.8	2.9	0.8	1.3
37	13	1,958	3 + 4	0	7.0	10.6	1.1	1.7
38	13	103	3 + 3	0	8.8	10.2	1.4	1.6
39	13	483	3 + 3	0	7.0	9.2	1.1	1.5
40	14	364	3 + 3	0	4.3	6.6	1.2	1.9
41	14	182	3 + 3	0	7.6	8.1	1.4	1.5
42	14	6,784	4 + 3	12	9.5	15.6	2.7	4.4
Mean		1,664.8		3.5	3.1	4.2	1.1	1.6
SD		2,721.2		6.7	2.1	2.9	0.4	0.7

DISCUSSION

^{11}C-choline PET has been successfully applied to visualize prostate cancer, bladder cancer, and several other solid malignancies (*6,23–26*). Previous ^{11}C-choline PET studies conducted in patients with primary prostate cancer have led to conflicting results. Although ^{11}C-choline has repeatedly been shown to visualize primary prostate cancer, the observed sensitivity for disease detection varied considerably (*6–8,17,26,27*). On the other hand, ^{11}C-choline was found to be rather successful for the detection of occult (low-volume) recurrent and distant metastatic disease (*11,28,29*). A clear understanding of the mechanisms involved in increased ^{11}C-choline uptake and retention by prostate cancer is still lacking. In light of these previous findings, our study was conducted to identify whether ^{11}C-choline PET would identify high-risk primary prostate cancer by rigorously comparing the ^{11}C-choline uptake with markers of aggressiveness such as the Gleason score and MIB-1/Ki-67 labeling index using 3D multimodality fusion with histology.

The major result of the current study indicates that increased ^{11}C-choline uptake in primary prostate cancer is correlated with histologic surrogate markers of aggressiveness. For our evaluation, we used the well-established Gleason score and the MIB-1/Ki-67 labeling index. Extensive literature exists showing that both are reliable prog-

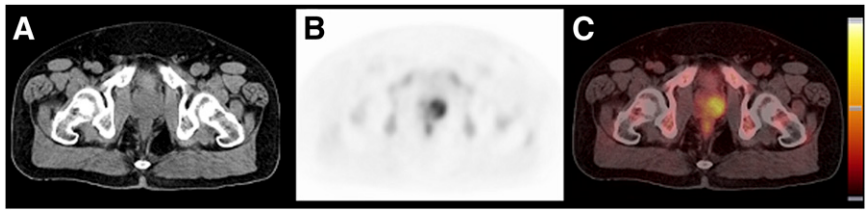

FIGURE 2. Non–contrast-enhanced CT (A), ^{11}C-choline PET (B), and rigid fusion image (C) of patient 14 with adenocarcinoma of prostate on left side. PET images are scaled to SUV, with minimum at −0.05 and maximum at 8. Note differences of apparent uptake when compared with registered ^{11}C-choline image in Figure 3.

nostic markers for prostatectomized patients (*13–15*). Many solid malignancies including lung, colon, breast, and prostate cancers overexpress choline kinase, which phosphorylates choline to phosphocholine as the first step of choline metabolism (*30*). Therefore, intracellular choline concentrations are determined by both choline transport and choline kinase activity (*31,32*). Choline kinase expression has been shown to be increased because of certain cell stresses and the presence of important oncogenes, which therefore influence cell membrane synthesis because choline is a major constituent of mammalian cell membranes (*33*). As a result, the rapid growth and proliferation of cancer cells may lead to increased membrane or fatty acid demands. Using a panel of tumor cell lines, Yoshimoto et al. confirmed in cell culture experiments that the ^{14}C-choline uptake is positively correlated with DNA synthesis (*32*).

Our data seem to contradict earlier reports showing that ^{11}C-choline uptake did not differentiate between grade and stage of prostate cancer or even between malignancy and benign prostatic hyperplasia (*9,27*) and the study from Breeuwsma et al., who were the first to directly compare the uptake of ^{11}C-choline with immunohistochemical cell proliferation markers in prostate cancer lesions (*34*). Lacking true colocalization between PET and histologic parameters, which restricted all these studies to the exclusive investigation of apparently ^{11}C-choline–positive lesions, the studies evaluated whether the intensity of visual uptake and mean tumor SUV obtained from ^{11}C-choline PET correlated with Gleason score, T-stage, and—in the case of Breeuwsma et al.—nuclear MIB-1/Ki-67 staining. Thus, ^{11}C-choline–negative lesions were not included in their analysis. Because of the inability to definitively localize nonmalignant prostate tissue on ^{11}C-choline PET, tumor-to-background ratios were also not available for analysis. It is not surprising that previous studies failed to identify significant correlations, considering differences in technique, patient populations, and small sample sizes in most studies and expected variability of histologic and imaging parameters. In fact, our results do not truly dispute these prior findings, because our results merely predict that most ^{11}C-choline–positive lesions (as identified by $T_{(mean)}$/B and $T_{(max)}$/B ratios), compared with ^{11}C-choline–negative lesions, have a Gleason score greater than or equal to 4 + 3 and display moderately increased MIB-1/Ki-67 staining.

Reske et al. reported more promising results in 26 patients with pT2a to pT4 primary prostate cancer as they unambiguously located tumor lesions, visually and semiquantitatively, using an SUV threshold of 2.65 (*26*). Although they were unable to demonstrate a correlation of the tumor SUV with the Gleason score, they found a significant correlation with the T stage. Our results further indicate that the mean tumor SUV (as used by Sutinen et al. (*9*), Breeuwsma et al. (*34*), and Reske et al. (*26*)) and the maximum tumor SUV (as used by Farsad et al. (*17*)) are poor predictors of Gleason score and MIB-1/Ki-67 labeling index, whereas normalization by nonmalignant prostate tissue clearly improves lesion characterization. In fact, on the basis of our data the ratio between tumor and normal tissue is the key to identifying aggressive disease, whereas the absolute mean or maximum SUV in a given lesion has less predictive value. This observation is critical because it

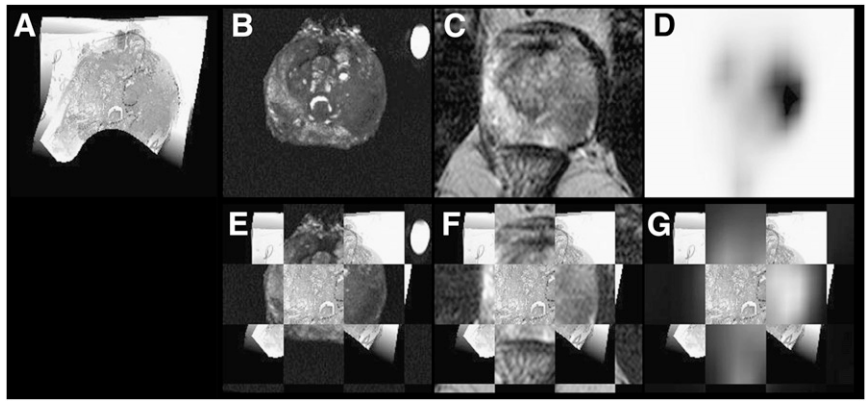

FIGURE 3. Registration of specimen MRI (B), anatomic transpelvic coil MRI (C), and ^{11}C-choline PET (D) imaging onto 1 gray-scale–converted whole-mount histology slice (A) for patient 14. Cancerous tissue is encircled in dotted lines on histology by pathologist. Alternating checkerboard fusion of registered specimen (E), transpelvic MRI (F), and registered PET imaging (G) with histology is displayed in second row. On histology, posterior aspect of histology slice leaves imaging plane of MRI and PET and is therefore not visualized (black).

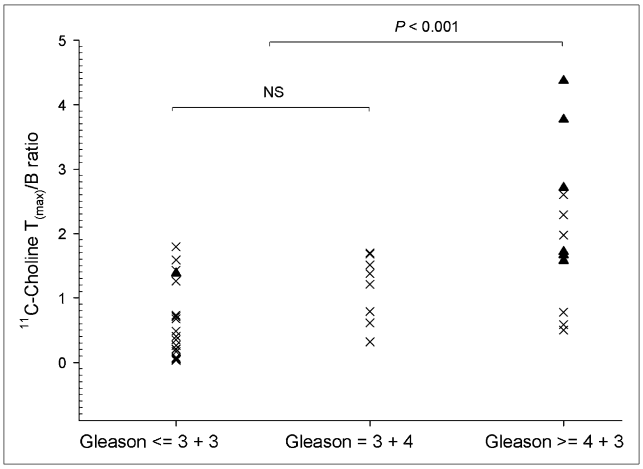

FIGURE 4. ^{11}C-choline $T_{(max)}$/B ratio differentiated tumors with Gleason score of 4 + 3 or higher vs. 3 + 4 and lower ($P < 0.001$); however, ratio failed to distinguish Gleason 3 + 4 vs. 3 + 3 and lower (NS). Tumor lesions with MIB-1/Ki-67 labeling index of 5 or higher are shown as ▲, and all other lesions are shown as × ($n = 42$). NS = not statistically significant.

highlights the considerable variability of ^{11}C-choline uptake in benign prostate tissues (as seen in our patient population), which raises the possibility of additional (unknown) parameters unrelated to malignant progression systematically influencing prostatic ^{11}C-choline biodistribution or metabolism.

Without coregistered histology, normalization of tumor uptake by nonmalignant prostate tissue is difficult because the true location of benign prostate tissue is not definitely known. This is especially problematic given the identified variability of ^{11}C-choline uptake within the benign prostate (central vs. peripheral gland) and when considering that prostatitis and hormonal treatment might have variable effects on the uptake of benign and malignant tissues. Biologic characterization of prostate cancer using ^{11}C-choline may, however, be possible using coregistration with high-resolution anatomic imaging (such as T2-weighted MRI). As current state-of-the-art MRI of prostate cancer improves (*35*), future clinical hybrid PET/MRI will benefit lesion characterization by providing reliable anatomic image information, verifying (or disproving) the existence of a tumorous lesion at the site of focally increased ^{11}C-choline uptake. If confirmed, such a lesion could—at the same time—be metabolically characterized by ^{11}C-choline as being higher or lower risk. Hybrid PET/MRI may even include MRI spectroscopy, which recently has also shown promise in the identification of aggressive disease (*36*).

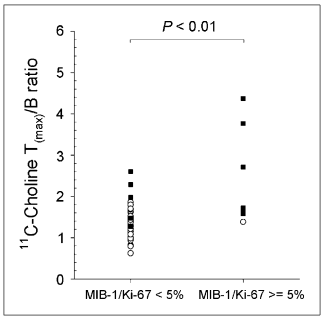

FIGURE 5. ^{11}C-choline $T_{(max)}$/B ratio differentiated tumor lesions with MIB-1/Ki-67 labeling index of 5 and higher vs. 4 and lower ($P < 0.01$). Tumor lesions with Gleason score of 4 + 3 or higher are shown as ■, and all other lesions are shown as ○ ($n = 42$).

Our approach included the registration of multiple imaging modalities (including MRI) using a mutual-information system and TPSs to accomplish 3D, nonlinear (warping) deformations. Additional coregistration of histologic information was possible after breaking up the difficult direct registration of histology and in vivo imaging into achievable subregistration tasks involving intermediate ex vivo block-face photography and specimen MRI. This methodology was recently introduced and evaluated by our group (*12*). Although such multimodality registration tasks are not without intrinsic errors (between 2.3 and 3.7 mm as determined earlier by Park et al. (*12*)), properly registered fusion images are certainly more accurate than simply comparing ^{11}C-choline PET or PET/CT images with individual histologic slices. In fact, given the considerable deformations in specimen extraction and processing, the likelihood that a 2-dimensional histologic sample maps directly back into a 2-dimensional plane of a given in vivo image volume seems incredibly small (*37*).

Several previous studies investigating primary prostate cancer with ^{11}C-choline PET reported cases with false-positive findings; however, we did not observe focally increased ^{11}C-choline uptake in benign tissues. Although precise spatial correlation with pathology was not available, earlier studies attributed such false-positive foci to the overlap of benign tissue with malignancy (*10*), high-grade prostate intraepithelial neoplasm, or prostatitis (*17*). Because the ^{11}C-choline uptake is known to be influenced by inflammation, false-positive results may also have been biopsy-induced when biopsies were performed close to PET (*26*).

On the basis of data obtained in this study, important reasons for the failure to characterize primary prostate cancer reliably using ^{11}C-choline PET are the lack of proper coregistration of histology with PET and partial-volume effects. Even with normalization of ^{11}C-choline data using $T_{(mean)}$/B and $T_{(max)}$/B ratios, we found considerable overlap of 4 aggressive low-volume cancers with nonmalignant tissues. Most patients were imaged on a PET/CT scanner with a reconstructed resolution of approximately 9 mm (we purposely used identical reconstruction settings on the second high-resolution scanner to maintain comparability). Although such performance characteristics are currently not uncommon, they are insufficient to characterize low-volume disease. Using partial-volume correction algorithms will likely not overcome this limitation and improve lesion detection because the expected uptake differential is relatively low (approximately 2–4 times higher in aggressive lesions than in contralateral benign tissue as seen in our study). Also, such algorithms assume

homogeneous tracer uptake in both the lesion and its vicinity (*38*). Systematic information about heterogeneity of ^{11}C-choline uptake in prostate cancer is not available, but our study and others (*26*) demonstrated regional differences of ^{11}C-choline uptake within benign prostatic tissues. An additional confounding factor for peripheral zone lesions is the temporal variation of extraprostatic activity in the rectum, which is not well represented on fusion MRI as performed in this study.

Evidence of extracapsular tumor is a strong predictor of metastases and prostate cancer death (*1*). Although we were unable to directly identify capsular penetration or invasion of the seminal vesicles by visual inspection of ^{11}C-choline PET images, most ^{11}C-choline–positive lesions constituted as T3 disease. On the basis of our data, T3 (or higher) disease should be suspected if focally enhanced ^{11}C-choline uptake is identified within a known cancer lesion. Coregistration with high-resolution MRI might provide further evidence to support the presence of T3 disease.

Definitive treatment cannot be recommended for all patients with localized prostate cancer. Therefore, accurate differentiation between low or intermediate versus highly aggressive prostate cancer early in the disease process is important for clinical decision making. It is clear from the Scandinavian report that prostatectomy mainly benefits men younger than 65 y with higher summed Gleason scores at or above 7 (*1*), but it does not suggest that definitive treatment would be inappropriate for aggressive early-stage disease for men older than 65 y. Because of extensive PSA testing, many men are classified as having prostate cancer of Gleason score less than 6 at diagnosis, and whether such disease requires treatment is a highly controversial issue (*2,39*). The accurate identification of aggressive lesions is a requirement for the adoption of active surveillance as described by Dall'Era et al. (*40*), commonly done by repeated prostate biopsies. Yet noninvasive imaging approaches would considerably facilitate such surveillance (watchful waiting) if they prove to have accuracy equal to or greater than repeated multiple random biopsies. However, we caution that before ^{11}C-choline (or other molecular markers of prostate cancer aggressiveness) can be integrated into diagnostic algorithms providing guidance for treatment pathways, additional prospective verification is needed to support that bioptic sampling of ^{11}C-choline–positive lesions is clinically feasible and is at least as accurate as random prostate biopsies. This would necessitate the fusion of ^{11}C-choline uptake data with high-resolution anatomic imaging to identify lesions for targeted biopsy.

CONCLUSION

Our preliminary data indicate that increased ^{11}C-choline uptake in primary prostate cancer normalized by nonmalignant prostate tissue may serve as a marker of tumor aggressiveness. Even after necessary confirmation of our pilot data in a larger series of patients, the difficulties in identifying benign prostatic tissues without sophisticated fusion techniques will limit clinical applications. It is, however, conceivable that improved imaging equipment offering fusion of ^{11}C-choline PET data with high-resolution anatomic imaging (such as future hybrid PET/MRI) may offer the potential to guide targeted prostate biopsies and to noninvasively select high-risk patients for definitive treatments such as surgery or radiotherapy.

ACKNOWLEDGMENTS

We thank the staff of the PET and MRI suites for their excellent technical support. We also honor our coinvestigator Dr. Saroja Adusumilli, who died in a car accident in March 2007 at the age of 36, for her outstanding contributions to this research and dedication to patient care. This research is supported by P50 CA069568 NIH/NCI (Prostate Cancer SPORE).

REFERENCES

1. Bill-Axelson A, Holmberg L, Filen F, et al. Radical prostatectomy versus watchful waiting in localized prostate cancer: the Scandinavian prostate cancer group-4 randomized trial. *J Natl Cancer Inst.* 2008;100:1144–1154.
2. Albertsen PC. A challenge to contemporary management of prostate cancer. *Nat Clin Pract Urol.* 2009;6:12–13.
3. Cookson MS, Fleshner NE, Soloway SM, Fair WR. Correlation between Gleason score of needle biopsy and radical prostatectomy specimen: accuracy and clinical implications. *J Urol.* 1997;157:559–562.
4. Fleshner NE, Cookson MS, Soloway SM, Fair WR. Repeat transrectal ultrasound-guided prostate biopsy: a strategy to improve the reliability of needle biopsy grading in patients with well-differentiated prostate cancer. *Urology.* 1998;52:659–662.
5. Podo F. Tumour phospholipid metabolism. *NMR Biomed.* 1999;12:413–439.
6. Hara T, Kosaka N, Kishi H. PET imaging of prostate cancer using carbon-11-choline. *J Nucl Med.* 1998;39:990–995.
7. Kotzerke J, Prang J, Neumaier B, et al. Experience with carbon-11 choline positron emission tomography in prostate carcinoma. *Eur J Nucl Med.* 2000;27:1415–1419.
8. de Jong IJ, Pruim J, Elsinga PH, Vaalburg W, Mensink HJ. Visualization of prostate cancer with ^{11}C-choline positron emission tomography. *Eur Urol.* 2002;42:18–23.
9. Sutinen E, Nurmi M, Roivainen A, et al. Kinetics of [^{11}C]choline uptake in prostate cancer: a PET study. *Eur J Nucl Med Mol Imaging.* 2004;31:317–324.
10. Scher B, Seitz M, Albinger W, et al. Value of ^{11}C-choline PET and PET/CT in patients with suspected prostate cancer. *Eur J Nucl Med Mol Imaging.* 2007;34:45–53.
11. Krause BJ, Souvatzoglou M, Tuncel M, et al. The detection rate of [^{11}C]choline-PET/CT depends on the serum PSA-value in patients with biochemical recurrence of prostate cancer. *Eur J Nucl Med Mol Imaging.* 2008;35:18–23.
12. Park H, Piert MR, Khan A, et al. Registration methodology for histological sections and in vivo imaging of human prostate. *Acad Radiol.* 2008;15:1027–1039.
13. Laitinen S, Martikainen PM, Tolonen T, Isola J, Tammela TL, Visakorpi T. EZH2, Ki-67 and MCM7 are prognostic markers in prostatectomy treated patients. *Int J Cancer.* 2008;122:595–602.
14. May M, Siegsmund M, Hammermann F, Loy V, Gunia S. Prognostic significance of proliferation activity and neuroendocrine differentiation to predict treatment failure after radical prostatectomy. *Scand J Urol Nephrol.* 2007;41:375–381.
15. Aaltomaa S, Karja V, Lipponen P, et al. Expression of Ki-67, cyclin D1 and apoptosis markers correlated with survival in prostate cancer patients treated by radical prostatectomy. *Anticancer Res.* 2006;26:4873–4878.
16. Herzog H, Tellmann L, Hocke C, Pietrzyk U, Casey M, Kuwert T. NEMA NU2-2001 guided performance evaluation of four Siemens ECAT PET-scanners. *IEEE Nucl Sci Symp Conf Rec.* 2003;4:2836–2838.

17. Farsad M, Schiavina R, Castellucci P, et al. Detection and localization of prostate cancer: correlation of ^{11}C-choline PET/CT with histopathologic step-section analysis. *J Nucl Med.* 2005;46:1642–1649.
18. Meyer CR, Boes JL, Kim B, et al. Demonstration of accuracy and clinical versatility of mutual information for automatic multimodality image fusion using affine and thin-plate spline warped geometric deformations. *Med Image Anal.* 1997;1:195–206.
19. Shah R, Bassily N, Wei J, et al. Benign prostatic glands at surgical margins of radical prostatectomy specimens: frequency and associated risk factors. *Urology.* 2000;56:721–725.
20. Shah R, Mucci NR, Amin A, Macoska JA, Rubin MA. Postatrophic hyperplasia of the prostate gland: neoplastic precursor or innocent bystander? *Am J Pathol.* 2001;158:1767–1773.
21. Mehra R, Han B, Tomlins SA, et al. Heterogeneity of *TMPRSS2* gene rearrangements in multifocal prostate adenocarcinoma: molecular evidence for an independent group of diseases. *Cancer Res.* 2007;67:7991–7995.
22. Fleming ID, Cooper JS, Henson DE. *AJCC Cancer Staging Manual.* 5th ed. Philadelphia, PA: Lippincott-Raven; 1997.
23. Hara T, Kosaka N, Shinoura N, Kondo T. PET imaging of brain tumor with [methyl-^{11}C]choline. *J Nucl Med.* 1997;38:842–847.
24. Picchio M, Treiber U, Beer AJ, et al. Value of ^{11}C-choline PET and contrast-enhanced CT for staging of bladder cancer: correlation with histopathologic findings. *J Nucl Med.* 2006;47:938–944.
25. Hara T, Inagaki K, Kosaka N, Morita T. Sensitive detection of mediastinal lymph node metastasis of lung cancer with ^{11}C-choline PET. *J Nucl Med.* 2000;41:1507–1513.
26. Reske SN, Blumstein NM, Neumaier B, et al. Imaging prostate cancer with ^{11}C-choline PET/CT. *J Nucl Med.* 2006;47:1249–1254.
27. Giovacchini G, Picchio M, Coradeschi E, et al. [^{11}C]choline uptake with PET/CT for the initial diagnosis of prostate cancer: relation to PSA levels, tumour stage and anti-androgenic therapy. *Eur J Nucl Med Mol Imaging.* 2008;35:1065–1073.
28. Picchio M, Messa C, Landoni C, et al. Value of [^{11}C]choline-positron emission tomography for re-staging prostate cancer: a comparison with [^{18}F]fluorodeoxyglucose-positron emission tomography. *J Urol.* 2003;169:1337–1340.
29. Reske SN, Blumstein NM, Glatting G. [^{11}C]choline PET/CT imaging in occult local relapse of prostate cancer after radical prostatectomy. *Eur J Nucl Med Mol Imaging.* 2008;35:9–17.
30. Glunde K, Bhujwalla ZM. Choline kinase alpha in cancer prognosis and treatment. *Lancet Oncol.* 2007;8:855–857.
31. Plathow C, Weber WA. Tumor cell metabolism imaging. *J Nucl Med.* 2008;49(suppl 2):43S–63S.
32. Yoshimoto M, Waki A, Obata A, Furukawa T, Yonekura Y, Fujibayashi Y. Radiolabeled choline as a proliferation marker: comparison with radiolabeled acetate. *Nucl Med Biol.* 2004;31:859–865.
33. Janardhan S, Srivani P, Sastry GN. Choline kinase: an important target for cancer. *Curr Med Chem.* 2006;13:1169–1186.
34. Breeuwsma AJ, Pruim J, Jongen MM, et al. In vivo uptake of [^{11}C]choline does not correlate with cell proliferation in human prostate cancer. *Eur J Nucl Med Mol Imaging.* 2005;32:668–673.
35. Wang L, Mazaheri Y, Zhang J, Ishill NM, Kuroiwa K, Hricak H. Assessment of biologic aggressiveness of prostate cancer: correlation of MR signal intensity with Gleason grade after radical prostatectomy. *Radiology.* 2008;246:168–176.
36. Zakian KL, Sircar K, Hricak H, et al. Correlation of proton MR spectroscopic imaging with Gleason score based on step-section pathologic analysis after radical prostatectomy. *Radiology.* 2005;234:804–814.
37. Meyer CR, Wahl RL. Image fusion. In: Wahl RL, ed. *Principles and Practice of PET and PET/CT.* 2nd ed. Philadelphia, PA: Lippincott, Williams & Wilkins; 2009:111–116.
38. Aston JA, Cunningham VJ, Asselin MC, Hammers A, Evans AC, Gunn RN. Positron emission tomography partial volume correction: estimation and algorithms. *J Cereb Blood Flow Metab.* 2002;22:1019–1034.
39. Albertsen PC, Hanley JA, Fine J. 20-year outcomes following conservative management of clinically localized prostate cancer. *JAMA.* 2005;293:2095–2101.
40. Dall'Era MA, Cooperberg MR, Chan JM, et al. Active surveillance for early-stage prostate cancer: review of the current literature. *Cancer.* 2008;112:1650–1659.